Modelling and Results for an Array of 32 Oscillating Water Columns.

Thomas Kelly*, Thomas Dooley†, John Campbell‡ and John Ringwood*
*Department of Electronic Engineering
National University of Ireland, Maynooth, Co. Kildare, Ireland
E-mail: thomas.e.kelly.2012@nuim.ie
E-mail: john.ringwood@eeng.nuim.ie
† Dundalk Institute of Technology, Dublin Rd., Dundalk, Ireland
E-mail: thomas.dooley@dkit.ie
‡Wave Energy Ireland, Unit F1 Nutgrove Office Park,Rathfarnham, Dublin 14, Ireland
E-mail: info@waveenergyireland.ie

***Abstract*—As part of an investigation into the feasibility of an offshore combined wind/wave energy converting platform, comprising one or more wind turbines mounted on a floating structure in which a number of oscillating water columns (OWCs) are embedded, testing was carried out on a 1:50 scale model of the wave energy converting component of the platform. The model comprises two legs joined at one end at an angle of 90 degrees. A form of soft latching is implemented through the use of high and low-pressure plenums to which the OWC chambers communicate via air admittance valves. The model was tested in a number of configurations, subject to varying amounts of simulated power take-off damping and over a range of incident regular-wave periods. Platform motions, OWC chamber and plenum pressure and water column motions were recorded for each test. This paper discusses some considerations in the design, construction, instrumentation and testing of the model. Thermodynamic theory describing the flow of air throughout the system, based on the conservation of mass, is developed and related to the motion of the water columns. Representative results from the model testing in the time domain are presented. Finally, some conclusions are drawn from these results.**

***Index Terms*—oscillating water column, latching, passive control, combined wind/wave, scale modelling**

I. Introduction

Combining wind and wave energy converting apparatus in an offshore environment presents the developer with a number of advantages. While ocean waves can be viewed as a wind-driven phenomenon, the correlation between the occurrence of conditions suitable for wind energy conversion and those suitable for wave energy conversion is not always strong [1]. Thus, by combining the two forms of electrical generation, the variation in power output from a single location can be reduced. Further, economic benefits for the developer can arise by using a shared infrastructure for the two means of power generation. For this reason, a number of combined wind/wave energy converting systems are under development, and the work outlined here concerns one such concept. This concept envisages a large floating platform comprising two legs arranged in a 90-degree, V configuration. This configuration is illustrated in Figure 1, which shows a 3-dimensional representation of the platform

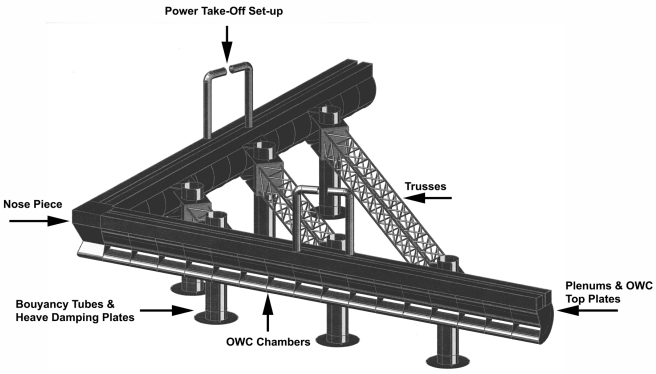

Fig. 1. Dimensionally accurate AutoCad model of platform

model. The wave energy component is based on a development of the classic oscillating water column (OWC) concept. Cross trusses between the two legs of the V-shaped platform provide the necessary structural strength, and the platform has been designed in accordance with the relevant Det Norske Veritas (DNV) codes [2]. A single point floating production storage and offloading unit (FPSO) style mooring located at the nose of the V allows the platform to weathervane into the direction of the incident waves. As currently envisaged, a single, large, offshore horizontal axis wind turbine is to be located at this nose. This location will ensure that the turning moments acting on the platform due to the reaction of the wind force on the turbine will be kept to a minimum to eliminate the danger of such moments turning the platform beam-on to the incident waves and also to prevent such moments rotating the platform out of the desired alignment with the incident waves when the wind and wave headings are not identical. Each leg of the platform incorporates a number of chambers with side openings to allow ingress of seawater to create a column of water within the chambers. These openings are located on the outside of the V of the platform so that the action

of incident waves results in motion of these water columns. During operation, for all wave regimes, these openings remain below the water level, and the chambers convert the energy stored in the motion of the incident waves into pneumatic energy, which can be further converted into electric energy using an air-driven turbine. The current concept envisages sixteen chambers in each leg, the size of each chamber being equal and determined based on the typical North Atlantic wave regime and the hydrodynamic characteristics of the resulting water column. The dividing walls between the chambers are at 90 degrees to the back wall of the leg, and hence at 45 degrees to the incident waves when the platform is aligned into the incident waves as described. Two individual pressure plenums run along the length of each leg of the platform – thus, a total of four pressure plenums are included. Each chamber is connected to the two plenums on the corresponding leg via airflow conduits. Passive air admittance valves allow for air to flow in one direction only between the chambers and the plenums. One plenum on each leg operates at a pressure higher than atmospheric, and collects high-pressure air that is generated by the upward movement of the water column in a chamber. Note that air will only flow into this plenum from a chamber if the air pressure within the chamber is greater than that within the plenum. The second plenum operates at a pressure lower than atmospheric. Air will flow from this plenum into a chamber due to the downward motion of the water column in the chamber if the pressure within the chamber is lower than that within the plenum. Should the pressure within a chamber at any time be less than that within the high-pressure plenum while also being greater than that within the low-pressure plenum, neither valve will open, and no flow of air between the chamber and the plenums will take place. This will result in the height of the water column remaining virtually locked, though some movement will take place due to the compressibility of the air within the chamber. This arrangement shares characteristics with that investigated by Lopes et al. [3]. Such action comes under the broad term latching, and is passive in nature. The purpose of latching is to align the phase of the exciting force due to the incident wave and the phase of the velocity of the water column motion. It is based on a force threshold method, the theory of which is discussed by Falcão [4], [5]. The two plenums on one leg are to be connected to allow air to flow between the high-pressure plenum, through a pneumatic turbine, and into the low-pressure plenum. Thus, in terms of the air flow, the chambers and plenums of one leg are a closed system.

II. Scale Model

A 1:50 scale model of the proposed platform was constructed. While the full-scale platform would likely be constructed from reinforced concrete, this scale model was constructed primarily from stainless steel. Each leg of the model platform is 4.9 metres in length. Perspex windows were included to allow visual inspection of the motion of the water column in each chamber during the testing. Buoyancy tubes, to which heave damping plates were installed, fit through the connecting trusses, and these can be installed and removed to test the model in different configurations. Likewise, removable wave-guide vanes can be installed on the lower edge of the chamber openings, and can be removed. In order to simulate a power take-off (PTO) arrangement and introduce varying levels of damping to the system, the high- and low-pressure plenums on each leg were connected to each other using 76 mm diameter stainless steel tubes. These tubes rise vertically from the plenums to a height of 600 mm before turning through 90 degrees to face each other. A gap of 200 mm is left between these tubes to allow for the installation of Venturis of varying throat diameters. These Venturis were constructed from glass-reinforced plastic, and an airtight seal between the Venturis and the model obtained using latex couplers. Once the model was complete, a range of tests was performed to ensure the system was airtight and watertight where required. Figure 1 shows a 3-dimensional schematic of this model as in configuration 4, see Table I below. This drawing is dimensionally accurate, and allows the mass and centre of gravity of the model to be determined using the AutoCAD 'massprop' command. These quantities were required for use with the motion capture system used to track the six rigid body modes of motion of the platform. Wave probes were installed in all chambers along one leg of the model to record the motion of the water columns during the testing. These probes are located along the vertical centre line of the chambers. Pressure transducers were likewise installed in these chambers to record the variation in chamber air pressure during the testing. More pressure transducers were installed to record the pressure at both ends and at the centre point of each plenum. Two further pressure sensors were located at the midpoints of the PTO simulating pipes on either side of the Venturi, as described above, to allow for airflow calculations through the Venturis, and hence allow power absorption calculations to be performed. A Pitot tube was also installed in the PTO arrangement to measure the airflow velocity beyond the Venturi to confirm the results obtained using standard Venturi theory, but this quickly became blocked during the testing and was not used further. Motion capture equipment was used to determine the rigid body motions of the platform. A number of further wave probes were installed in the OWC chambers of the second leg to compare the results

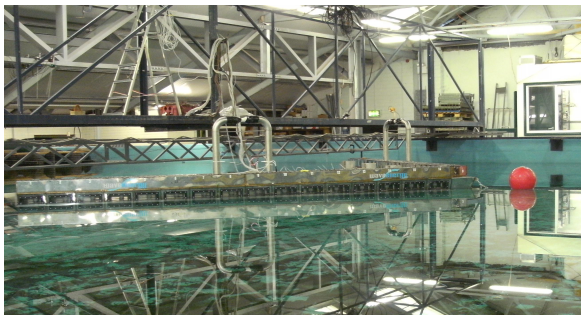

Fig. 2. 1:50 scale model installed at the Ocean Basin in the HMRC prior to comencement of testing

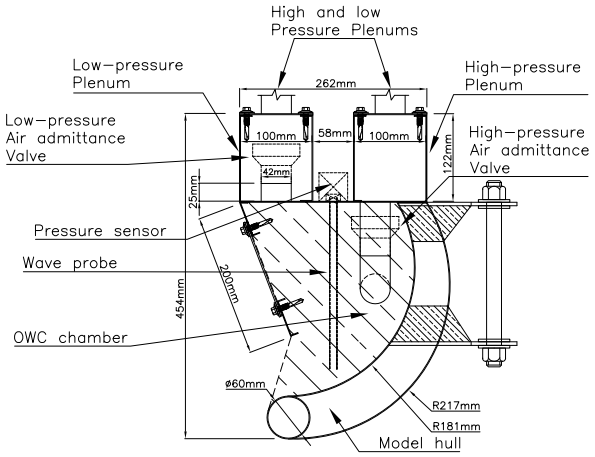

Fig. 3. Cross-section of oscillating water column and plenum arrangement

obtained from both legs. However, due to limits on the number of channels that could be monitored at the test facility and the expense involved, the second leg was not as extensively instrumented as the first, and no pressure transducers were installed in the OWC chambers of this leg. A total of 22 wave probes and 28 pressure transducers were installed on the model.

The cross-sectional profile of the platform chambers is curved in profile to reduce losses due to vortex formation, and this is reflected in the model. Figure 3 illustrates the cross-section through one chamber of the model, and further illustrates the location of the plenums, the wave probe and the pressure transducer for this chamber.

III. Model Testing

The model was installed in the large ocean basin at the Hydraulics and Maritime Research Centre (HMRC) located at University College Cork, Ireland. It was moored using a single point catenary style arrangement where an anchored chain was connected to the nose of the V. The model was free to rotate about this point, simulating a single point FPSO-style mooring. Using lead weights, the draft of the model was set as required, and the centre of gravity, mass and moments of inertia determined using the AutoCAD model. All sensors were connected to the data acquisition system, which samples at a rate of 32 Hz, and calibrated. The model was then tested for a variety of configurations, with a range of damping conditions achieved through varying Venturi throat diameters for a range of wave conditions. This paper discusses the results of testing in the time domain for regular waves: thus, while some irregular wave conditions were simulated using Bretschneider spectra, these results are not included as part of this study.

With reference to the model outlined in Section II, testing was carried out in five configurations, in sequence, as outlined in Table I. Each configuration was tested for a range of regular waves of 60 mm wave height for wave periods of 0.71, 0.85, 0.99, 1.13, 1.27, 1.41, 1.56, 1.70, 1.84 and 1.98

TABLE I
Test configurations

Configuration 1	The model is fitted with the buoyancy tubes/heave damping plates and with the lower wave-guide vanes
Configuration 2	The buoyancy tubes/heave damping plates are removed, and the platform is fitted with the lower wave-guide vanes
Configuration 3	The buoyancy tubes/heave damping plates and lower wave-guide vanes are removed
Configuration 4	The buoyancy tubes/heave damping plates are re-installed with the addition of larger heave damping plates made from a near neutrally buoyant material of water plane area equal to that of the lower wave-guide vanes
Configuration 5	As for configuration 4 with the lid of the low-pressure plenums removed

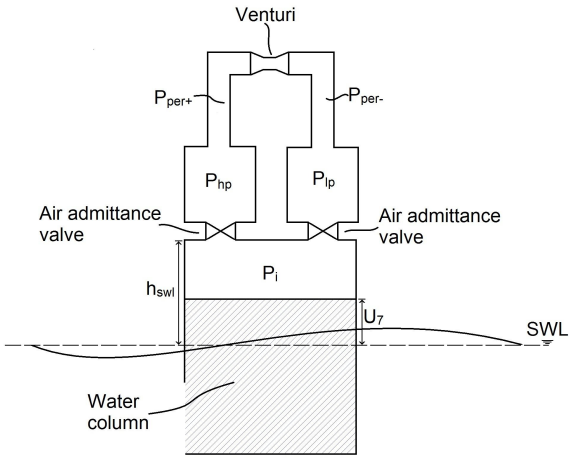

Fig. 4. Schematic of one OWC chamber, the high- and low-pressure plenum and the conduit including Venturi

seconds, equivalent to a full scale wave height of 3 metres and full scale wave periods of 5, 6, 7, 8, 9, 10, 11, 12 and 13 seconds respectively, with each test running for 60 seconds to allow any transient affects to pass. For Configuration 1, the model was tested using Venturis of throat diameter equal to 15 mm, 20 mm, 22.5 mm, 25 mm, 27.5 mm and 30 mm. Following an analysis of the power absorbed by the model during this stage of the testing, the remaining configurations were tested for throat diameters of 20 mm, 22.5 mm, 25 mm and 30 mm. A large volume of data was thus obtained and was subsequently analysed using the MATLAB programming environment. Some representative sample results are presented in Section V and discussed in Section VI.

IV. Theory

Figure 4 illustrates a schematic of a single OWC chamber connected to a high- and a low-pressure plenum via air admittance valves. The high- and low-pressure plenums are in

turn connected via a conduit, in which is located an air flow restriction in the form of a Venturi. The system is considered to comprise of a number of volumes in which the air pressure is assumed to be constant throughout at any instant in time, and varying with respect to time. These volumes comprise of the air trapped above the water column in each chamber, the air within the high pressure plenum and the section of conduit leading from the high-pressure plenum to the Venturi and finally the air within the section of conduit from the Venturi to the low-pressure plenum combined with that in the low-pressure plenum itself. The theory initially developed did not assume that a plenum and associated conduit could be considered as one volume; however the results of this testing as shown in Section V demonstrate the validity of this assumption, allowing for considerable simplification of the theory at this scale.

Consider the chamber to be fixed in all rigid body modes and that the water column is operating in heave only while interacting with a high and low-pressure plenum. The equation of motion of the water column in the frequency domain is given as:

$$[m + a]\,\ddot{U} + b\,\dot{U} + c\,U = F_e - (P_i - P_{pl})A_{owc} \qquad (1)$$

where m in the mass of the water column, a is the frequency dependent added mass of the water column, b is the frequency dependent radiated damping of the water column and c is the hydrostatic stiffness of the water column. F_e is the frequency dependent exciting force in the heave mode of the water column, P_i is the air pressure in the OWC chamber above the water column, P_{pl} is the air pressure in a plenum and A_{owc} is the cross-sectional area of the water column chamber. U, $\dot{U}$ and $\ddot{U}$ are the displacement, velocity and acceleration of the heave motion of the water column respectively.

As described earlier, when subject to an incident ocean wave, the water column may operate in one of three modes:

1) If the pressure within the OWC chamber is greater than that in the high-pressure plenum, air will flow from the chamber into that plenum.
2) If the pressure within the OWC chamber is lower than that in the low-pressure plenum, air will flow from that plenum into that chamber.
3) If the pressure within the chamber is less than that in the high-pressure plenum and greater than that in the low-pressure plenum, no air will flow between the chamber and either plenum, effectively latching the water column.

The equation of motion of the water column will vary depending upon in which of the modes the water column is operating. When operating in the first mode described above and henceforth referred to as the 'discharge' mode, this equation in the time domain, after Cummins [6], becomes:

$$[m + a(\infty)]\ddot{U} + \int_{-\infty}^{t} K(t-T)\dot{U} + \phi(t) + c\,U + (P_{hp} - P_i)A_{owc} = F_e(t) \qquad (2)$$

In the above equation, $a(\infty)$ is the so called infinite frequency added mass, the convolution integral $\int_{-\infty}^{t} K(t-T)\dot{U}$ incorporates the memory effects of the fluid, $\phi(t)$ denotes the non-linear viscous force and P_{hp} is the air pressure in the high-pressure plenum. The non-linear viscous force, $\phi(t)$, may be determined using Morison's Equation, see, for example [7]. Similarly, when the water column is operating in the second mode above, henceforth referred to as the 'suction' mode, the following equation of motion applies:

$$[m + a(\infty)]\ddot{U} + \int_{-\infty}^{t} K(t-T)\dot{U} + \phi(t) + c\,U + (P_i - P_{lp})A_{owc} = F_e(t) \qquad (3)$$

Here, P_{lp} represents the air pressure in the low-pressure plenum. Assigning the subscripts i to denote the i^{th} OWC chamber, hp the high-pressure plenum and PTO conduit and lp the low-pressure plenum and conduit, the ideal gas law can be applied to each chamber and the two plenums and conduits on either side of the Venturi as follows:

$$\frac{P_i V_i}{RT} = m_i \qquad (4)$$

$$\frac{P_{hp} V_{hp}}{RT} = m_{hp} \qquad (5)$$

$$\frac{P_{lp} V_{lp}}{RT} = m_{lp} \qquad (6)$$

where P denotes the absolute pressure of a volume of gas, V represents the volume occupied by the gas, R is the gas constant, T is the temperature of the gas and m is the mass of the gas in a volume. The hydrodynamic quantities of Equations (2) and (3) may be determined using numerical solvers such as WAMIT [8]. Given that each leg is comprised of sixteen chambers and the two plenums with associated conduit, in order to determine all the pressures and water column displacements when the platform is stationary, it is necessary to construct a system of 34 coupled equations to solve for the 16 water column displacements, the pressure within the 16 OWC chambers and the pressure within the high and low-pressure plenums.

Considering first the pressure within the i^{th} chamber, differentiating Equation (4) with respect to time yields:

$$\frac{RT}{V_i}\frac{\partial m_i}{\partial t} + \frac{m_i R}{V_i}\frac{\partial T}{\partial t} = \frac{\partial P_i}{\partial t} + \frac{P_i}{V_i}\frac{\partial V_i}{\partial t} \qquad (7)$$

If the process within the OWC chamber is considered to be reversible and adiabatic, then the following relationship may be applied:

$$P_i V_i^{\gamma} = constant \qquad (8)$$

where γ is the heat capacity ratio, $\approx$1.4 for air. If this equation is combined with Equation (4), the following relationship is established:

$$P_i^{1-\gamma} T_i^{\gamma} = constant \qquad (9)$$

Performing a logarithmic differentiation on Equation (9) results in the following equation:

$$\frac{P_i}{T}\frac{\partial T}{\partial t} = \frac{\gamma - 1}{\gamma}\frac{\partial P_i}{\partial t} \tag{10}$$

By substituting Equation (10) into Equation (7) and using the relationship $c^2 = \gamma RT$ where c is the speed of sound in air, the following relationship can be established:

$$\frac{c^2}{V_i}\frac{\partial m_i}{\partial t} = \frac{\partial P_i}{\partial t} + \gamma\frac{P_i}{V_i}\frac{\partial V_i}{\partial t} \tag{11}$$

This result was obtained by Gervelas et al. [9] when considering an OWC open to atmosphere and independently by Hazem et al. [10] who performed an analysis on a pneumatically actuated system based on the Energy equation. As the water column is modelled as a piston, the two systems can be considered analogous. Now, when the water column is operating in discharge mode, $\Delta P = P_{hp} - P_i$, and thus:

$$\frac{\partial P_i}{\partial t} = \frac{\partial P_{hp}}{\partial t} - \frac{\partial \Delta P}{\partial t} \tag{12}$$

The mass flow rate when the OWC is operating in discharge mode with respect to the chamber is negative, i.e:

$$\frac{\partial m_i}{\partial t} = -\dot{m}_i \tag{13}$$

For the purposes of clarity in this derivation, it is assumed that the volume of air in the chamber can be reasonably approximated by the height of volume of air by the cross-sectional area of the chamber and that this cross-sectional area does not vary for small water column displacements. (With reference to Figure 3, it can be seen that for this model this cross-sectional area will vary, and it will be necessary to take account of this variation in the numerical model.) For a chamber of non-varying cross-sectional area, the height of the volume of air is the height of the volume at still water conditions, h_{swl}, minus the displacement of the water column, U Thus, the volume of air is given by:

$$V_i = A_{owc}\left(h_{swl} - U\right) \tag{14}$$

Substituting Equations 12, 13 and 14 into Equation (11) yields:

$$\frac{\partial \Delta P}{\partial t} = \frac{c^2}{A_{owc}\left(h_{swl} - U\right)}\dot{m}_i + \frac{\partial P_{hp}}{\partial t} - \frac{\gamma P}{\left(h_{swl} - U\right)}\frac{\partial U}{\partial t} \tag{15}$$

Once the coefficient of discharge, C_D, the edge distance, L_g, and the opening height of the diaphragm, h_{max} for a valve are known, the mass flow rate across the valve can be expressed in terms of the pressure difference across it as [11]:

$$\dot{m}_i = C_D L_g h_{max}\sqrt{2\rho_{air}\Delta P} \tag{16}$$

Substituting Equation (16) into Equation (15) leads to:

$$\frac{\partial \Delta P}{\partial t} = \frac{c^2}{A_{owc}\left(h_{swl} - U\right)}C_D L_g h_{max}\sqrt{2\rho_{air}\Delta P} + \frac{\partial P_{hp}}{\partial t} - \frac{\gamma P}{\left(h_{swl} - U\right)}\frac{\partial U}{\partial t} \tag{17}$$

By differentiating Equation (5), a similar result to Equation (7) may be obtained. Note, that in this instance, as the volume of the plenum is constant there is no ∂V/∂t term:

$$\frac{\gamma RT}{V_{hp}}\frac{\partial m_{hp}}{\partial t} = \frac{\partial P_{hp}}{\partial t} \tag{18}$$

The mass flow rate into and out of the high-pressure plenum is the sum of flows into the plenum from all chambers operating in discharge mode minus the flow out of the plenum through the Venturi, i.e:

$$\frac{\partial m_{hp}}{\partial t} = \sum \dot{m}_i^{discharge} - \dot{m}^{vent} \tag{19}$$

where $\dot{m}^{vent}$ is the flow out of the high-pressure plenum across the Venturi. Note that any chambers operating in suction mode do not contribute to this mass flow rate. $\dot{m}^{vent}$ is in turn given by:

$$\dot{m}_{vent} = C_D A_V\sqrt{2\rho\left(P_{hp} - P_{lp}\right)} \tag{20}$$

In Equation (20), C_D is the coefficient of discharge for the Venturi, A_V is the cross-sectional area of the Venturi throat. The pressure drop across the Venturi is the difference between the pressures in the high- and low-pressure sides of the PTO arrangement.

The mass flow rate for the low-pressure plenum, $\dot{m}_{lp}$ is likewise the mass flow into the low-pressure side from the Venturi minus the flow out of the plenum into those OWC chambers operating in suction mode, and the mass flow rate into those chambers from the low-pressure plenum may be expressed mathematically as in Equation (16). The final required equation is derived from the fact that the total mass of air in one leg, m_T is constant at all times as the system is closed, and thus the sum of all airflows is equal to zero, i.e.:

$$\frac{\partial m_T}{\partial t} = \sum \dot{m}_i^{discharge} - \sum \dot{m}_i^{suction} - \dot{m}_{vent} = 0 \tag{21}$$

Note that when operating in suction mode, Equation (3) applies and the mass flow $\dot{m}_i$ will be into the OWC chamber and hence have the opposite sign to when a chamber is operating in discharge. For a chamber that is latched, the change in pressure is equal to the change in exciting force divided by the water column area, and $\dot{m}_i = 0$. This theory may be extended to include the six rigid body motions of the platform. When implemented as a numerical model, the decision as to which of Equations 2 and 3 is to be used for a time step will depend on the pressures as determined from the previous time step.

One further aspect of the theory necessary to interpret the results presented in this paper is the means by which the power absorbed by the model platform from the incident waves during the testing was calculated. For fluid flow, power is the product of the volumetric flow rate, Q, and the pressure, P. The time series of the volumetric flow through the Venturi may be determined by dividing the time series of the mass flow rate through the Venturi by the density of air. The mass flow rate across the Venturi is given by Equation (20) The

time series of the power absorbed by one leg of the model platform for a particular test run is:

$$Pow_{av} = \left(\frac{\dot{m}_{vent}}{\rho_{air}}\right)\left(P^{+}_{per} - P^{-}_{per}\right) \tag{22}$$

The average power absorbed for the leg is the root mean square of the volumetric flow rate by the root mean square of the pressure difference. Note that the average power per metre wave front in the incident wave can be found from the following equation:

$$Pow_{wave} = \frac{\rho_w g^2 A^2}{4\omega} \tag{23}$$

where g is the acceleration due to gravity, A is the incident wave amplitude, ρ_w is the density of water and ω is the incident wave frequency.

V. Time Domain Results

Figure 5 illustrates the variation in pressure with respect to time of four of the installed pressure sensors. These sensors were located at either end and at the horizontal midpoint of one of the high-pressure plenums, and at the vertical midpoint of the corresponding PTO conduit. The sample results in Figure 5 were taken from the test run with the model as in Configuration 1 at an incident wave period of 1.41 seconds with a Venturi diameter of 15 mm. Figure 6 illustrates the corresponding data for the low-pressure side for the same time frame.

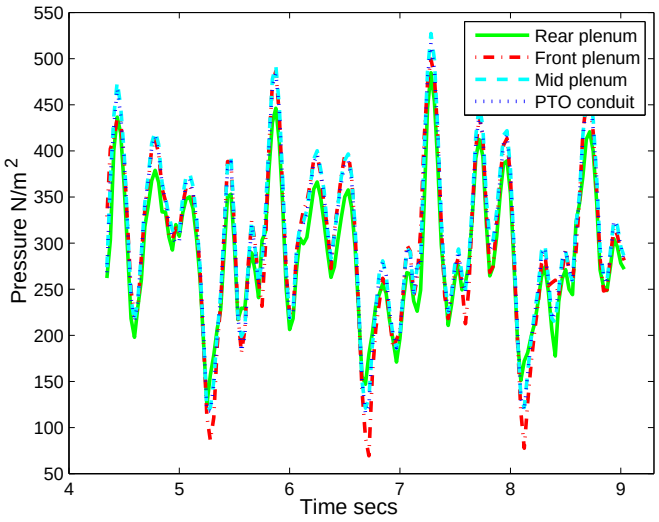

Fig. 5. Time series of pressure at either end and at the horizontal midpoint of the high-pressure plenum, and the vertical midpoint of the high-pressure PTO conduit

Figure 7 shows the variation in pressure and water column height within an OWC chamber (in this instance the ninth chamber from the stern of the platform) and the variation in pressure within the high- and low-pressure plenums with respect to time when the model was subjected to an incident wave period of 1.41 seconds with Venturis of 25 mm throat diameter installed. In this figure, the green and brown dashed lines represent the pressure and water column height within

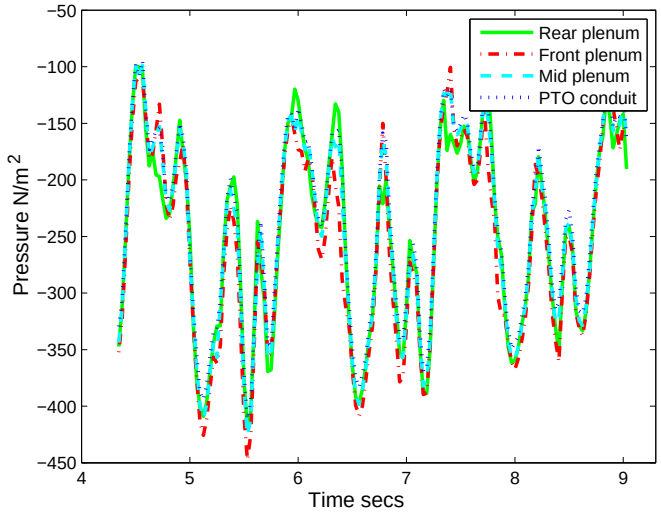

Fig. 6. Time series of pressure at either end and at the horizontal midpoint of the low-pressure plenum, and the vertical midpoint of the low-pressure PTO conduit

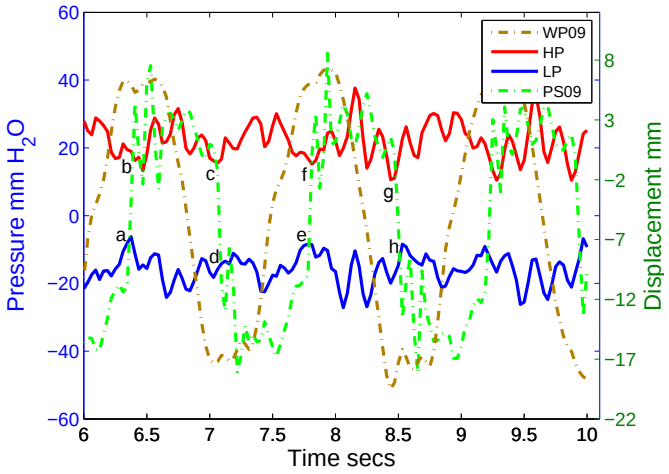

Fig. 7. Time series of the variation of pressure and water column height in the ninth OWC chamber, and the pressure in the high- and low-pressure plenums with respect to time

the chamber respectively, and the red and blue solid lines represent the variation of pressure within the high- and low-pressure plenums respectively. Figure 8 illustrates the water column displacement relative to the platform with respect to time for the water column in chamber 1, located at the stern of the model. The data was taken from a test run where the model was set up as in Configuration 2 in Table I with the 25 mm throat diameter Venturi set installed and with the model subject to an incident wave of a period of 0.99 seconds. The latching of the water column can clearly be seen in this figure. For example, between a time of approximately 29.6 and 30.1 seconds into the test run, and again at 30.6 and 31.25 seconds, such latching is clearly apparent. The form of this latching on the upwards motion of the water column closely matches that as illustrated by Falnes [12].

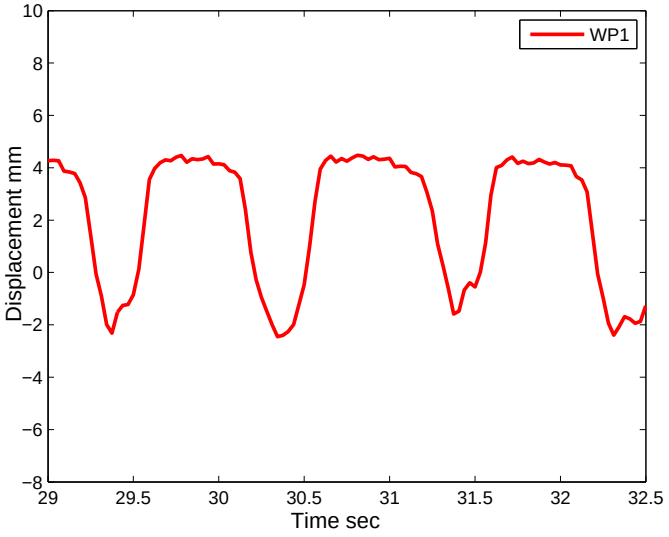

Fig. 8. Time series of the variation of the relative height of the water column in OWC chamber 1, illustrating the latching effect

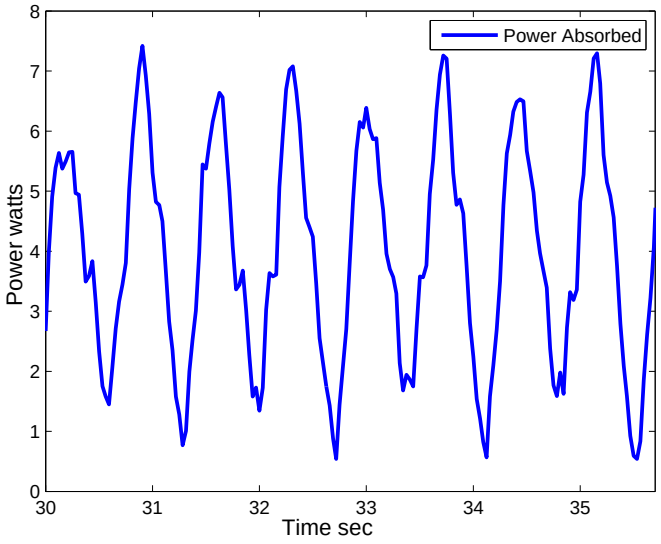

Fig. 10. Time series of instantaneous power absorbed by one leg of the model

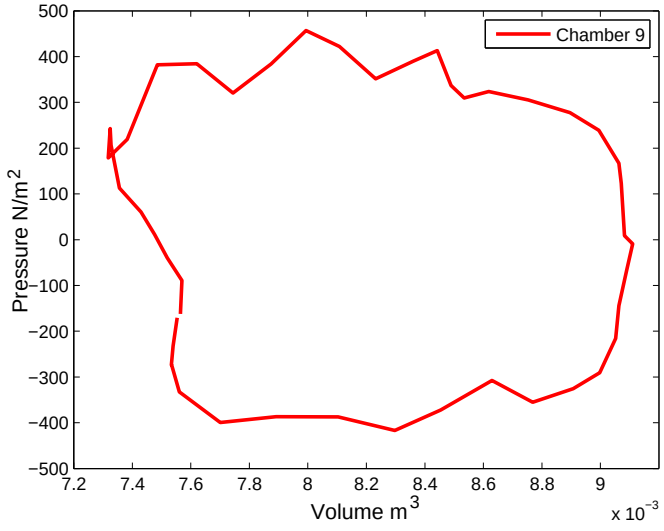

Fig. 9. Pressure-Volume plot for chamber 9

Figure 9 illustrates a Pressure-Volume plot for chamber 9 with the model setup as in Configuration 1 using the 25 mm throat diameter Venturi set and an incident wave period of 1.41 seconds. This plot illustrates the relationship between the pressure in the air above the water column in an OWC chamber and the volume of that air over one full wave period, and hence one period of oscillation, of the water column. The pressure is the gauge pressure within the chamber as measured by the pressure transducer, and the volume of the air cavity is determined from the wave probe signal. Figure 10 illustrates the instantaneous power absorbed by one leg of the model platform setup as in Configuration 1 in Table I with the 25 mm throat diameter Venturi set installed while subject to an incident wave of 30 mm amplitude at 1.41 second period determined as outlined in Section IV. A total of four incident wave periods will have contacted the model during the time period illustrated in this figure. The average power absorbed by the leg during the test run illustrated in Figure 10 is 4.02 Watts. Given that the model is in communication with 6.9 metres of wave front, the platform in this configuration and subject to this wave absorbs 24% of the power in the wave. The maximum percentage of wave power absorbed by the model during these tests was achieved with the model as in Configuration 4 and was approximately 37%. Work outside the scope of this report has demonstrated that the model platform as tested here is over-damped, and significant improvements on the percentage power absorbed from the waves can be achieved. With respect to the rigid body motions of the platform itself, as would be expected, the amount of movement in roll, sway and yaw is minimal, with the motion in surge limited to the platform slowly moving away from the direction of the incident waves until restrained by the mooring. Thus, the main modes of motion of interest are the pitch and heave motions of the platform. While such motions may be either beneficial to the power absorbed by the platform or parasitic to it, such motions will have implications for the accelerations experienced by any wind turbines that may be installed, and are thus undesirable. Figure 11 illustrates the pitch motion of the platform for the setup which exhibited the greatest amount of pitching motion. This run occurred with the model setup as Configuration 3 with the 20 mm Venturi set installed and with the model subject to an incident wave period of 1.84 seconds. As can be seen from this figure, the pitch angle of the platform varied with a range of approximately ± 2.25 degrees from the neutral position. However, it should be noted that the range of pitching motion between the various configurations for incident waves of equal periods is not large. For example, with an incident wave of 1.98 seconds, the pitch motion of the platform varied between ± 1.5 degrees for the platform as in Configurations 1 and 2, and 2 degrees with the

model in Configuration 3. Figure 12 illustrates the greatest degree of heave motion of the platform recorded, in this case for the model as in Configuration 1 using the 15 mm throat diameter Venturis in response to an incident wave of 1.98 seconds. This Venturi set was not used in conjunction with any other model configurations as listed in Table I as they were found to absorb the lowest level of power during the initial testing. The heave motion in Figure 12 can be seen to vary between approximately ± 20 mm. Typical heave motion ranges for the various remaining setup and Venturi pairings were in the ± 15 mm range for this incident wave frequency. Both the pitch and heave motions of the platform reduce significantly as the incident wave period decreases, and, for example, at an incident wave period of 0.99 seconds, the heave motion typically had a range of ± 2 mm from the neutral position, and the pitch motion typically had a range of ± 0.1 degree.

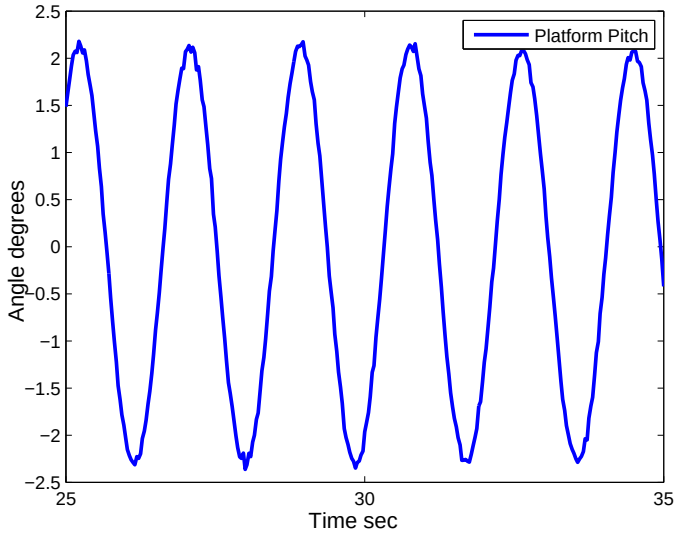

Fig. 11. Time series of platform pitching motion

While Figures 7 and 8 are useful in illustrating the general concept behind the intended operation of the platform, and are by no means unique, they were specifically chosen due to their suitability for illustrating the points discussed in Section VI below. They do not, however, illustrate all of the complexity inherent in the operation of the platform. When compared to earlier, smaller-scale testing that was conducted on a three-chamber fixed platform model, it is clear that increasing the number of interacting chambers and allowing the platform itself to operate in the standard six rigid body modes greatly increases the complexity of the processes at work. For example, consider Figure 13 which illustrates the complete time series for the water column displacement in OWC chamber 17 with respect to the platform with the model setup in Configuration 1 using the 25 mm throat diameter Venturi set with an incident wave period of 0.99 seconds. For much of this test run, the water column oscillates about a point approximately 10 mm above the still water level in a relatively uniform fashion. However, between approximately

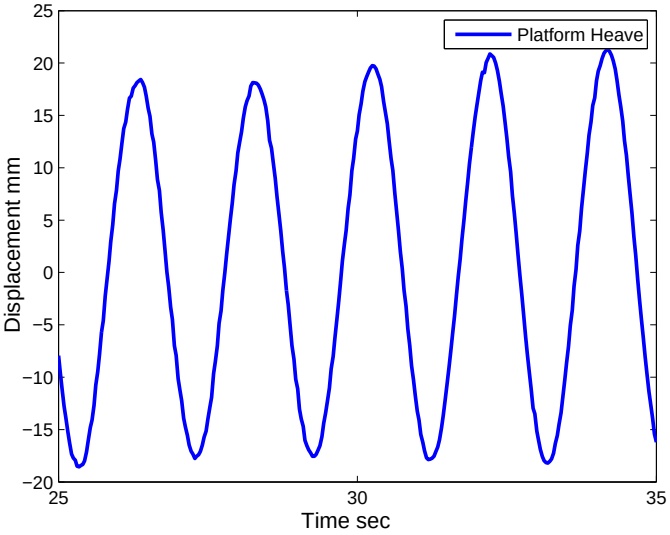

Fig. 12. Time series of platform heaving motion

25 and 40 seconds into the test run, the mean level of the water column increases to about approximately 20 mm about the still water level, and the amplitude of the oscillation decreases dramatically. However, as the dominant period of the water column oscillations during this time is equal to that of the incident wave, such a reduction in the amplitude of oscillation is unlikely to be due to the latching effect outlined previously (the small, higher-frequency oscillations within the main peaks may be the result of the latching effect). Once past this time, the nature of the oscillations returns to a more regular motion. Contrast this with the motion of the water column in OWC chamber 13 as illustrated in Figure 14 for the same test run. No such unusual changes in behaviour are observed in this instance, but note the behaviour of the water column between approximately 15 and 20 seconds, where the amplitude of the wate column motion did change due to the complexity of the system. There are several possible explanations for the behaviour of the relative water column motion in chamber 17 during this test run. It is possible that the coupled motion of the platform and the water column was such so as to result in this relative motion of the water column at that time. It is also possible, however, that the air admittance valve in the low-pressure plenum became stuck, preventing the water column moving down relative to the platform during this section of the test run.

VI. Discussion

Consider first the assertion made in Section IV that the pressure within a plenum and the corresponding PTO simulating conduit can be considered uniform at any instance in time at the scale at which the scale model testing was conducted. As can be seen from Figures 5, a close correlation exists between the pressures recorded by the three sensors in the high-pressure plenum and PTO conduit with respect to time. Likewise a similar correlation exists for the high-pressure plenum and

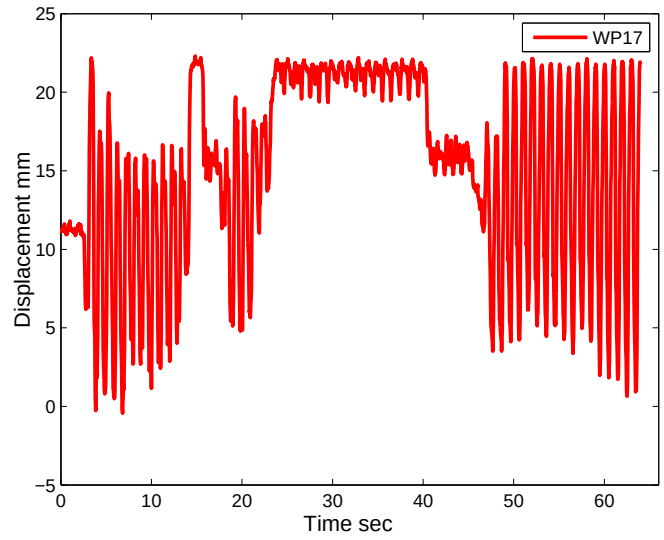

Fig. 13. Time series of the variation of the relative height of the water column in chamber 17

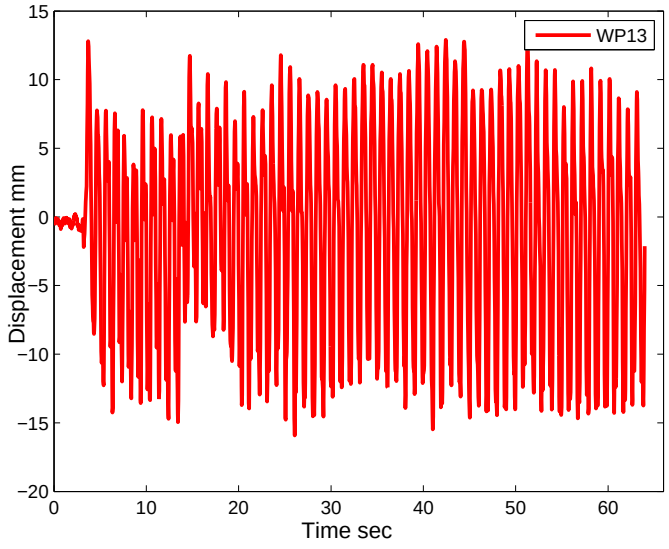

Fig. 14. Time series of the variation of the relative height of the water column in chamber 13

PTO conduit as shown in Figure 6. This match exists for all model configurations and damping levels currently tested at this scale.

While Figures 5 and 6 show that the assumption that the pressure is uniform throughout the plenum and PTO conduit is reasonable at this scale, this is not likely to be the case at larger scales. Theory such as that in Section IV may be extended to include mass flow balances between a plenum and a PTO conduit by considering a coefficient of discharge through the orifice between the plenum and the conduit. The theory may be further expanded to consider variations of pressure within the plenum. However, if the scale of the plenum is such that the pressure difference within it is significant, modelling such pressure variation accurately may require the use of finite element techniques.

Consider now the operation of one chamber over one period of an incident wave as shown in Figure 7. In the region to the left of the point labelled ‘a’, it can be seen that the pressure within the chamber is below that within the low-pressure plenum. The water column at this time in moving upwards relative to the chamber. This is possible as the pressure within the chamber does not exceed that in the low-pressure plenum. At the point labelled ‘a’, the pressure within the chamber exceeds that within the low-pressure plenum. At this time the pressure within the chamber rapidly increases between point ‘a’ and the point labelled ‘b’, to a value greater than the pressure within the high-pressure plenum. This increase from less than 20 mm H_2O below the initial chamber pressure to more than 30 mm H_2O takes place over $1/16^{th}$ of a second. The water column ceases to move upwards at point ‘a’ while the pressure within the chamber increases to that at point ‘b’. Between ‘b’ and point ‘c’, the pressure within the chamber fluctuates about that in the high-pressure plenum, and while the exciting force of the water column is in the positive direction, the water column motion reflects this. Before ‘c’, the direction of the water column exciting force reverses, and the water column itself begins to drop relative to the platform. In the reverse of the case when the pressure is below that in the low-pressure plenum before point ‘a’, the water column may move down relative to the platform as long as the pressure within the chamber remains above that in the high-pressure plenum. The pressure within the chamber drops below that in the high-pressure plenum for the final time in this cycle at point ‘c’, and the chamber pressure drops rapidly between points ‘c’ and ‘d’ in the same fashion as it increased between points ‘a’ and ‘b’ earlier in the cycle. Between ‘d’ and ‘e’, the pressure within the chamber is below that in the low-pressure plenum, and is equal to the pressure in the low-pressure plenum at point ‘e’, completing the cycle. It can be seen that this cycle repeats between points ‘e’, ‘f’, ‘g’ and ‘h’.

With reference to Figure 9, note how the pressure-volume plot forms a closed loop over a cycle and is similar in character to Pressure-Volume plots for reciprocating compressors as illustrated by, for example, Tramschek and MacLaren [13]. Much of the theory outlined in Section IV can equally be applied to such compressors. A large body of work exists in this area, and this plot would suggest that applying similar theory to this application in the time-domain as described may produce useful results.

Consider the instantaneous power absorbed by the model as illustrated in Figure 10. Note how the frequency of oscillation of the power absorbed is twice that of the incident wave oscillation, and this is true for all wave periods tested. The fact that the power oscillates at twice the frequency of the incident waves is a result of the use of the rectification of the air flows and is analogous to the output voltage from a diode bridge in response to an input of an AC voltage. At the scale of the current model, and as demonstrated by Figures 5 and 6, little compression of the air takes place within the plenums. However, at a larger scale it is envisaged that the

plenums will act in a manner analogous to a capacitor in an electrical rectifying circuit by temporarily storing absorbed power as compressed air and aid in the smoothing of the power absorption.

While the magnitude of the pitch and heave motions did not vary significantly between set ups and damping regimes, the phase of these motions to each other and the incident wave would vary. One important consequence of this was that in certain conditions the lips of the water columns at either end of the platform would breach the surface of the water. This would trap more air in the system, causing the platform to rise high in the water, exacerbating the breaching issue. This issue, along with other concerns regarding the likely hub height accelerations, will require further investigation. Both may be solved by reducing the platform heave and pitch motions, which in turn may be achieved in a number of ways, for example through the use of larger damping plates or by changing the platform water plane area and hence the natural frequencies of the platform.

VII. Conclusion

The primary purpose of the testing conducted on the 1:50 model was to investigate the effectiveness of the platform at absorbing power from incident waves, while at the same time investigating the overall stability of the platform with regard to the possible inclusion of one or more wind turbines, to determine the economic viability of the project. As such, less emphasis was placed on gathering data likely to be useful for the validation of numerical modelling. None the less, some useful information has been gathered for use with numerical models and some conclusions may be drawn with respect to the overall performance of the model.

With respect to the numerical model, the theory that was initially developed did not assume that the pressure within the plenums matched that within the PTO conduits on the high- and low-pressure sides, nor that the pressure was uniform throughout the plenums themselves. The results of this testing have shown that, at this scale, it is reasonable to assume uniform pressure throughout a plenum and the corresponding PTO conduit, and thus the theory to be applied to the numerical model in the time domain and presented herein has been significantly reduced in complexity. This will allow for a numerical model of the platform at this scale to be developed and validated in a reduced time frame. Further, useful information regarding the motions of the platform, the motions of the water columns and the pressure distribution throughout the system is now available to validate and refine the numerical model. Work on this numerical model is ongoing.

From a commercial perspective, it has been shown that, by using the technique described, the output from multiple floating OWCs may be manifolded and rectified in a reasonably efficient manner. Some issues do exist, notably the need for improved platform stability with regard to the inclusion of wind turbines on the platform while at the same time eliminating the issue of OWC chamber lips breaching the water surface. While concern has been raised with relation to the intermittent sticking of some air admittance valves, it is believed that this relates to the location of the valves, necessary due to the available space at this scale and is an issue that can be rectified at larger scales with relative ease. It has also been shown that the device in the configurations outlined here is over-damped with regard to the motions of the water columns. It is believed, however, that these issues can be overcome, and initial frequency domain models which are not the subject of this report would support this assertion. However, further testing will be required to confirm this assertion.

Acknowledgment

The experimental testing is part funded by the Sustainable Energy Authority of Ireland as part of the Ocean Energy Prototype Research and Development Programme under project number OC/OC/09/19681164. The authors wish to acknowledge the expertise and assistance given by the staff at the HMRC during the setup and testing of the 1:50 scale model. The first author further wishes to acknowledge the management of Wave Energy Ireland Ltd. for providing access to the model and testing process within the framework of research being undertaken pursuant to his Ph.D., and the Irish Research Council for providing funding for this research.

References

[1] F. Fusco, G. Nolan, and J. Ringwood, "Variability reduction through optimal combination of wind/wave resources – an irish case study." *Energy*, vol. 35, no. 1, pp. 314–325, 2010.

[2] D. N. Veritas, "Det norske veritas exchange [online catalogue]," http://exchange.dnv.com/publishing/ServiceDocs.asp, 2013.

[3] M. Lopes, J. Hals, R. Gomes, T. Moan, L. Gato, and A. O. Falcao, "Experimental and numerical investigation of non-predictive phase-control strategies for a point-absorbing wave energy converter." *Ocean Engineering*, vol. 36, no. 5, pp. 386–402, 2009.

[4] A. D. O. Falcao, "Modelling and control of oscillating–body wave energy converter with hydraulic power takeoff and gas accumulator." *Ocean Engineering*, vol. 34, no. 1, pp. 2021–2032, 2007.

[5] ——, "Phase control through load control of oscillatingbody wave energy converter with hydraulic power takeoff system." *Ocean Engineering*, vol. 35, no. 1, pp. 358–366, 2008.

[6] W. Cummins, *The Impulse Response Function and Ship Motions*, ser. Technical Report 1661. Department of the Navy, David Taylor Model Basin, 1962.

[7] S. Chakrabarti, *Hydrodynamics of Offshore Structures*. Computational Mechanics Publ., Southhampton, MA. USA, 1987.

[8] W. Inc., *WAMIT User Manual Version 7.0*. MA USA: WAMIT Inc, 2012, vol. 1.

[9] R. Gervelas, F. Trarieux, and M. Patel, "A time-domain simulator for an oscillating water column in irregular waves at model scale," *Ocean Engineering*, vol. 38, no. 8-9, pp. 1007–1013, 2011.

[10] A. I. Hazem, S. B. B. M. Noor, S. Bashi, and M. H. Marhaban, "Mathematical and intelligent modeling of electropneumatic servo actuator systems," *Australian Journal of Basic and Applied Sciences*, vol. 3, no. 4, pp. 3663–3671, 2009.

[11] R. A. Habing, "Flow and plate motions in compressor valves," Ph.D. dissertation, Twente University Holland, 2005.

[12] J. Falnes, *Principles for Capture of Energy from Ocean Waves. Phase Control and Optimum Oscillation*, ser. Technical Report. Department of Physics, NTNU, N-7034 Trondheim, Norway, 1995.

[13] A. Tramschek and J. MacLaren, "Simulation of a reciprocating compressor accounting for interactions between valve movement and plenum pressure chamber," in *International Compressor Engineering Conference Paper 356*, P. U. e Publications, Ed., West Lafayette, IN. USA, 1980.